Illumination Sensing in LED Lighting Systems Based on Frequency-Division Multiplexing

Hongming Yang, *Member, IEEE*, Jan W. M. Bergmans, *Senior Member, IEEE*, and Tim C. W. Schenk, *Member, IEEE*

***Abstract*—Recently, light emitting diode (LED) based illumination systems have attracted considerable research interest. Such systems normally consist of a large number of LEDs. In order to facilitate the control of such high-complexity system, a novel signal processing application, namely illumination sensing, is thus studied. In this paper, the system concept and research challenges of illumination sensing are presented. Thereafter, we investigate a frequency-division multiplexing (FDM) scheme to distinguish the signals from different LEDs, such that we are able to estimate the illuminances of all the LEDs simultaneously. Moreover, a filter bank sensor structure is proposed to study the key properties of the FDM scheme. Conditions on the design of the filter response are imposed for the ideal case without the existence of any frequency inaccuracy, as well as for the case with frequency inaccuracies. The maximum number of LEDs that can be supported for each case is also derived. In particular, it is shown that, among all the other considered functions, the use of the triangular function is able to give a better tradeoff between the number of LEDs that can be supported and the allowable clock inaccuracies within a practical range. Moreover, through numerical investigations, we show that many tens of LEDs can be supported for the considered system parameters. Remark on the low-cost implementations of the proposed sensor structure is also provided.**

***Index Terms*—Filter bank, frequency-division multiplexing, illumination sensing, LED illumination, Nyquist-1 functions.**

I. Introduction

DUE to the rapid development of solid-state lighting (SSL) technologies, high brightness light emitting diodes (LEDs) will play a major role in future indoor illumination systems. LEDs may largely replace incandescent and fluorescent lamps, mainly because of the advantages of LEDs such as high radiative efficiency, long lifetime, high tolerance to humidity, and limited heat generation [1], [2]. Considerable research interest, therefore, has been devoted to LED based illumination systems.

Manuscript received December 04, 2008; accepted April 07, 2009. First published June 10, 2009; current version published October 14, 2009. The associate editor coordinating the review of this manuscript and approving it for publication was Prof. Bogdan Dumtrescu. The material in this paper was presented in part at the IEEE International Conference on Acoustics, Speech, and Signal Processing (ICASSP), Taipei, Taiwan, R.O.C., April 19–24, 2009.

H. Yang is with the Department of Electrical Engineering, Eindhoven University of Technology, 5600 MB Eindhoven, The Netherlands, and also with Philips Research Eindhoven, The Netherlands (e-mail: h.m.yang@tue.nl).

J. W. M. Bergmans is with the Department of Electrical Engineering, Eindhoven University of Technology, 5600 MB Eindhoven, The Netherlands.

T. C. W. Schenk is with Philips Research Eindhoven, High Tech Campus 37, 5656 AE Eindhoven, The Netherlands.

Color versions of one or more of the figures in this paper are available online at http://ieeexplore.ieee.org.

Digital Object Identifier 10.1109/TSP.2009.2025091

LED-based illumination systems normally consist of a large number, e.g., hundreds, of spatially distributed LEDs. This is partly because a single state-of-the-art LED [3] still cannot provide sufficient illumination and also because extremely high brightness LEDs compromise eye safety.

Such spatially distributed LEDs, moreover, may be used to provide localized, dynamic and appealing lighting effects. To this end, the beam width of each LED is set to be narrow and the output illumination level of each LED is flexible. In practice, the illumination level of each LED is configured so that a desired lighting effect can be achieved at the location of interest, called *target location*.

In order to deliver different illumination levels, the output of each LED typically consists of repeatedly transmitted illumination pulses whose widths are modulated [4], so-called pulsewidth modulation (PWM), as illustrated in Fig. 1. The amplitude of the pulse train is called the *luminous flux* (in lumen), denoted by $a_{\mathrm{F},i}$, of the ith LED, and the duty cycle is denoted by p_i where $0 \leq p_i \leq 1$. The illumination level of the LED is represented by the product $a_{\mathrm{F},i}p_i$. In practice, the luminous flux of each LED is fixed, i.e., the illumination pulse train is binary, in order to maintain a high efficiency in the driver circuits. In contrast, the duty cycle of the illumination pulse train can be changed easily. Therefore, the level of output illumination is determined by the duty cycle of each LED. The resolution of the duty cycle thus determines the range of illumination levels that can be supported by a single LED. In an advanced illumination system [5], p_i is set in a logarithmic scale and each p_i can range from 10^{-3} to 1. Another key parameter of the PWM modulated pulse train is the frequency of the illumination pulses, also called the *fundamental frequency*, denoted by f_i for the ith LED. In general f_i should be high enough, e.g., higher than 200 Hz, so that no flicker can be perceived from an LED.

In the above discussions, we introduced how to make the illumination level of each LED flexible. Due to the large number of LEDs and the broad range of illumination levels that can be supported by each LED, the complexity to calibrate and control such a lighting system is quite high. To facilitate the control of such a high complexity system and be able to achieve engaging lighting effects, it is essential to be able to accurately estimate the illumination contribution of each individual LED at the target location. This process is named *illumination sensing* and is the focus of this paper. Further, for the purpose of illumination sensing, a sensor is located at the target location.

From the characteristics of the output of each LED, it is clear that the illumination component of each individual LED at the target location also consists of a PWM modulated pulse train,

except that the amplitude of the pulse train is now the *illuminance* (in lumen), denoted by $a_{\mathrm{I},i}$ for the ith LED, at the target location. The actual illumination contribution of an individual LED can be seen to be the product $a_{\mathrm{I},i}p_i$. Given the knowledge of p_i at the central controller, we in fact only need to estimate $a_{\mathrm{I},i}$ for all i, whose value is determined by the luminous flux of each LED and the free-space optical channel attenuation [6], [7].

Based on the illumination sensing results, various applications scenarios can be implemented in practice via the central controller. For instance, a user can copy the sensed lighting effect at the target location through the knowledge of the individual contribution of each LED and then recreate it somewhere else. This *copy and paste* application can also be repeated continuously as a user walks around. Many other application scenarios exist, however, it is beyond the scope of this paper to discuss more of these. In principle, there are two major operations of each application. One is the *sensing operation*, in which operation we estimate $a_{\mathrm{I},i}$ for all i. The other is the *illumination rendering operation*, when we set p_i to achieve the desired lighting effects. In order to realize the desired lighting effects in the second operation, it is important to obtain an accurate estimation of the illuminance of each LED, e.g., such that the estimation error compared to the actual value is invisible to human eyes, and within a short time, e.g., 0.1 second. Hence, there are two key application requirements to the sensing process, viz. accuracy and speed.

The light outputs from all LEDs simply sum up together at the target location. It is therefore difficult and expensive, if not impossible, to distinguish different LEDs optically. Instead, an electronic solution is desirable. Such a solution involves an optical-electrical converter, e.g., through a photodiode, at the target location to obtain an electrical pulse train. The electrical pulse train is again of similar shape as that illustrated in Fig. 1, except that the amplitude is now the *electrical current*, denoted by a_i for the ith LED. The ratio $\zeta_i \triangleq a_i/a_{\mathrm{I},i}$ (ampere/lumen), named the *responsitivity* of the optical-electrical conversion, is fixed and known for each LED, depending on the color of the LED. In this paper, we consider the case that all the LEDs are of the same color, i.e., ζ_i is independent of i. It is easy to extend the results obtained in this paper to the case when the colors of the LEDs are different. Therefore, we only need to estimate a_i for all i in the illumination sensing process. To this end, one may adapt or shape the illumination waveform of Fig. 1 individually for each LED, in such a manner that the contributions can be disentangled electronically. For instance, the illumination pulses in Fig. 1 can be intermitted with deterministic pulse trains that serve as identifiers for the LEDs. The intermitted ID pulses, however, may cause visible flicker. Whereas an approach was proposed in [6] and [7] without introducing visible flicker, reliable recognition of the distinct identifiers requires complex procedures to maintain synchronism among the LEDs and between the LEDs and the sensor. To avoid these disadvantages while maintaining low cost and low complexity driver circuits, in this paper, we consider a much simpler asynchronous approach that is based on frequency-division multiplexing (FDM). Here, all LEDs are operated at different yet fixed frequency f_i, with small yet easily discernible spacing, denoted by Δ_f, between the different frequencies.

The idea of setting the illumination pulse trains of the LEDs at distinct frequencies was proposed in [8]. In that paper, the research challenges, however, are quite different from those in this work. The reason is that [8] focused on a system with a small number of LEDs with an analog sensor structure in which the response time is not critical. In this paper, by contrast, we focus on a large number of LEDs and high-speed illumination sensing. Moreover, the performance limit of the FDM scheme is also studied. There is also an increasing interest in visible light communications using power LEDs, e.g., [2] and [9]. However, the objective of this paper is not to transmit data using visible light. On the contrary, there is actually no real data transmitted in our scheme.

The rest of this paper is organized as follows. A detailed discussion on the key system characteristics and requirements on illumination sensing is presented in Section II. The FDM scheme is introduced in Section III. Section IV characterizes the relation between the received electrical current at the sensor and the drive current of each LED. In Section V, we present a sensing approach while focusing on the fundamental frequency components in the received electrical current. In particular, three filter bank estimators with different design rationales are proposed. We further show that these three estimators can be viewed to be based on equivalent principles. In Section VI, the design of the filter responses for the proposed sensor structure is presented, through the performance investigation on both the ideal case without frequency inaccuracy and the worst case, in terms of $\{a_i, p_i\}$, with frequency inaccuracies. Finally, Section VIII concludes this paper.

II. System Characteristics and Requirements

In this section, we discuss the key system characteristics and requirements.

Number of LEDs: A state-of-the art LED can produce at most 200 lumen [3]. For an indoor environment, an illuminance level of about 400–1000 lux (lumen per m^2) is normally needed. Therefore, at least three to six LEDs per m^2 are necessary for an LED based illumination system. For instance, for a room with an area of 20 m^2, $L = 40$ to 100 LEDs are needed, where L denotes the number of LEDs. In practice, these LEDs are grouped into multiple modules with each module being controlled independently by the central controller. More independent LED modules are desirable since more degrees of freedom are available to give more flexible lighting effects. In this paper, we assume each LED can be controlled independently and investigate the maximum number LEDs that can be accommodated by the proposed illumination sensing scheme. In a practical implementation, each LED module can be viewed as a "hyper" LED and the results in this paper can thus also be applied there.

Accuracy of Illumination Sensing: To gauge accuracy in illumination sensing, we take human perception properties into consideration. The human visual system continuously adapts itself according to the background or environment lighting. Similarly, the *visibility* of an estimation error depends on the real

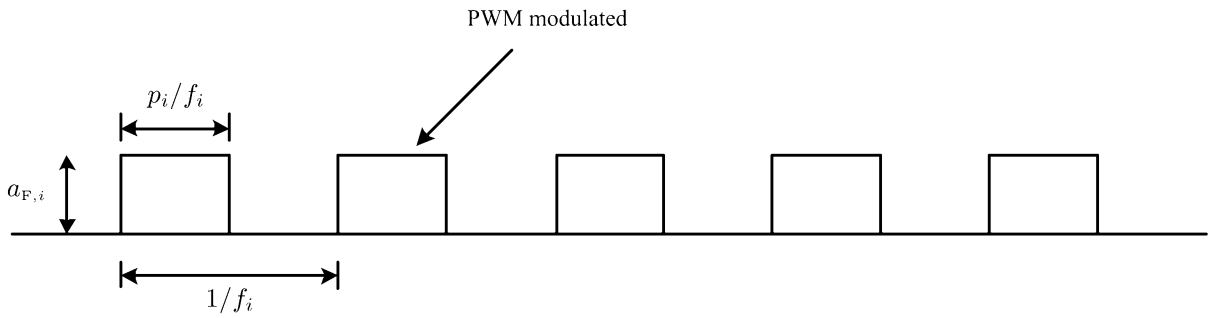

Fig. 1. PWM modulated illumination pulses to achieve flexible illumination levels. The amplitude of the pulse train is $a_{\mathrm{F},i}$ at the output of the ith LED, $a_{\mathrm{I},i}$ at the target location, and a_i at the output of an optical-electrical converter at the sensor.

illuminance level. Hence, in this paper, for a performance measure, we normalize the estimation error with respect to the real illuminance. Since the illumination contribution of the ith LED is equivalently characterized by $a_{\mathrm{I},i}p_i$, we propose to characterize the accuracy of illumination sensing with respect to the ith LED by

$$\xi_i \triangleq 10\log\left(\frac{|\hat{a}_{\mathrm{I},i}-a_{\mathrm{I},i}|p_i}{\sum_{m=1}^{L}a_{\mathrm{I},m}p_m}\right) = 10\log\left(\frac{|\hat{a}_i-a_i|p_i}{\sum_{m=1}^{L}a_m p_m}\right) \quad (1)$$

where $\hat{a}_i$ and $\hat{a}_{\mathrm{I},i}$ denote the estimated values for a_i and $a_{\mathrm{I},i}$, respectively. The nominator $|\hat{a}_{\mathrm{I},i}-a_{\mathrm{I},i}|p_i$ denotes the estimation error in terms of the illuminance contribution of the ith LED, while $\sum_{m=1}^{L}a_{\mathrm{I},m}p_m$ corresponds to the total illuminance contribution from all the LEDs at the target location. The second equation in (1) follows from $a_i=\zeta_i a_{\mathrm{I},i}$ and $\hat{a}_i=\zeta_i\hat{a}_{\mathrm{I},i}$. Hence, in practice, we only need to evaluate the performance of estimating a_i instead of $a_{\mathrm{I},i}$.

The exact value for $\xi_{\max}$ that defines the threshold for a visible error is dependent on many factors, e.g., the distance between a user and the sensor location. In general, from the experimental results in [10], when ξ_i is less than -20 dB, the estimation error is no longer visible to human eyes. Therefore, in this paper, we focus on the range of ξ_i that is above -20 dB. Note that -20 dB is only a lower bound for the ξ_i to be considered, while in certain practical situations, it might occur that an error ξ_i well beyond -20 dB may also be invisible.

If there are other light sources, e.g., sunlight or fluorescent lamps, in the environment, we may change the denominator of (1) into $\sum_{m=1}^{L}a_{\mathrm{I},m}+a_{\mathrm{I,other}}$, where $a_{\mathrm{I,other}}$ denotes the illuminance of these other light sources. The value of ξ_i is thus reduced by $10\log(1+a_{\mathrm{I,other}}/(\sum_{m=1}^{L}a_{\mathrm{I},m}))$. For the considered LED illumination system, there will be only a limited amount of light from other light sources, and hence the difference appears to be small. Moreover, ξ_i becomes smaller in the presence of other light sources, hence (1) can also be used as the worst-case performance measure.

High Speed Illumination Sensing: As for sensing speed, we may consider the tolerance time between the moment when a user pushes a button and that when the illumination level of a lamp is changed and enters a stable state. Another example concerns the normal speed of human movement such that a desired lighting effect can follow the user. In these cases, a *response time*, denoted by T, that is significantly below one second, is desired. More specifically, in this paper, we require $T\leq 0.1$ s.

Flicker Free Operation: As introduced in Section I, LEDs are switched on and off regularly. Thus, the output light signal from the LEDs consists of a principal component at the fundamental frequency, and the harmonics. The human visual system cannot perceive frequency components higher than 75 Hz in a stable situation. In other situations like rapid eye movement, higher frequency components up to a few hundred Hertz might also become visible. The visible frequency components result in an annoying flickering effect, which should be avoided. To stay well in the flicker free range, we require the fundamental frequency component of the light signals to be at least 200 Hz.

Low Cost Driver Circuits: There are also practical constraints on the driver circuits to maintain a low cost system. For instance, binary outputs are used for all LEDs, as illustrated in Fig. 1. Moreover, in an LED driver module, there is normally a crystal oscillator for the control unit to generate a train of square pulses at certain frequency. For a low cost design, the clock inaccuracy is assumed to be 100 parts per million (ppm). Besides the existing hardware, the extra cost at the LED driver circuits for the purpose of illumination sensing should be low to maintain a low complexity and low cost system.

III. Frequency-Division Multiplexing Scheme

In order to distinguish and estimate the illumination contribution from each LED, we can potentially choose to watermark the illumination pulse trains of the LEDs differently in terms of amplitude, frequency and/or phase. In view of the system characteristics and requirements introduced in Section II, we consider watermarking the *frequency* of the driver current in this paper, mainly because of the simplicity of this method. In this FDM scheme, the fundamental frequency f_i is set to be different for different i. Thus, the driver current of the ith LED can be represented by

$$s_i(t)=\sum_{n=-\infty}^{\infty}a_{\mathrm{S},i}\mathrm{rect}\left(\frac{t}{p_i/f_i}-t_i-n\frac{1}{f_i}\right) \quad (2)$$

where $a_{\mathrm{S},i}$ and t_i, where $-(1/2f_i)\leq t_i\leq(1/2f_i)$, denote the amplitude and the initial time shift of the driver current for the ith LED, respectively. The rectangular function $\mathrm{rect}(\cdot)$ is defined as $\mathrm{rect}(t)=1$ if $-1/2\leq t\leq 1/2$ and $\mathrm{rect}(t)=0$

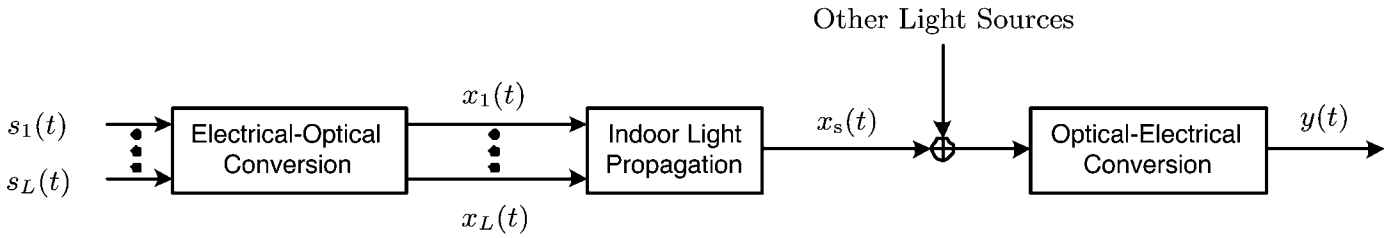

Fig. 2. Schematic for the channel model.

elsewhere. In response to $s_i(t)$, the illumination pulses at the output of the ith LED can be represented by

$$x_i(t) = \sum_{n=-\infty}^{\infty} a_{\mathrm{F},i} h_i\left(t - t_i - n\frac{1}{f_i}\right) \tag{3}$$

where the ratio $a_{\mathrm{F},i}/a_{\mathrm{S},i}$ is known as the *responsitivity* of the LED. The pulse function $h_i(t)$ is also approximately a rectangular function, except that there is some transient time, $\tau_{\mathrm{on},i}$ or $\tau_{\mathrm{off},i}$, at each ON-switch or OFF-switch operation. A more accurate description of $h_i(t)$ will be provided later in Section IV-A.

For this FDM scheme, with respect to the requirement on *low cost driver circuits*, we essentially only apply PWM as already used in conventional LED drivers, therefore there is actually no extra cost, beyond the existing hardware involved in the driver circuits.

The duty cycle p_i of each pulse train is set on a logarithmic scale [5] and we have $p_{\min} = 0.001 \le p_i \le 1$. However, the FDM scheme cannot work when $p_i = 1$, when the only frequency component is direct current (DC). Therefore, we can at maximum take the second largest value for p_i from [5], i.e., $p_{\max} = 0.97307$.

The frequency range of the FDM scheme is determined by the flicker-free requirement and the physical limit of the LEDs. As discussed in Section II, the fundamental frequency has to be larger than 200 Hz for the system to be flicker free. Moreover, in order to maintain $h_i(t)$ to be approximately rectangular for any p_i, we should also have $p_{\min}/f_i \ge \tau_{\mathrm{on}} + \tau_{\mathrm{off}}$. The response time $\tau_{\mathrm{on},i} + \tau_{\mathrm{off},i}$ is mainly determined by the coating phosphors if applied, and is expected to be less than 250 ns [4]. Hence, we get $f_{\mathrm{MAX}} = 0.001/(250 \times 10^{-9}) = 4$ kHz. In order to accommodate as many LEDs as possible and make sure that there is no possible overlap between f_i and the harmonics of any f_m where $m \ne i$, we take the frequency range to be 2 to 4 kHz. Hence, the bandwidth is $W = 2$ kHz. Moreover, frequency assignment is undertaken such that there is a uniform spacing Δ_f between the neighboring frequencies, i.e., $L = W/\Delta_f$. This spacing should be compatible with a low cost crystal oscillator with an accuracy of 100 ppm, for which the maximum frequency offset between an actual frequency and the corresponding ideal frequency is $10^{-4} f_i \le 0.4$ Hz. Later in this paper, we will study how many LEDs can be supported in practice by this FDM approach.

From above, using this FDM scheme, two challenges out of the five presented in Section II are already resolved, viz. flicker free operation and low-cost driver modules. In the rest of the paper, we will focus on the other three challenges. Before discussing the performance of sensing processing, we will first characterize the received signal at the sensor in the next section.

IV. Channel Model

In this paper, the channel model for the free-space indoor illumination system refers to the relation between the electrical current at the output of the photodiode at the target location, denoted by $y(t)$, and $s_i(t)$, i.e., the driver current of each LED. The channel response consists of three main components, i.e., the electrical–optical conversion, the indoor light propagation and the optical–electrical conversion. There are also disturbances in the channel. The schematic of the channel model is depicted in Fig. 2.

A. Electrical-Optical Conversion

The driver current of the ith LED consists of repeatedly transmitted rectangular pulses, as described in (2). The ith LED in turn performs the electrical–optical conversion, and generates the illumination pulses as represented in (3). Here, the pulse shape $h_i(t)$ consists of exponential ON-switch and OFF-switch ramps [11], and can be approximated as

$$h_i(t) = \begin{cases} 0, & t \le -\frac{p_i}{2f_i} \\ 1 - e^{-\frac{t+\frac{p_i}{2f_i}}{\tau_{\mathrm{on},i}}}, & -\frac{p_i}{2f_i} \le t \le \frac{p_i}{2f_i} \\ c_i e^{-\frac{t-\frac{p_i}{2f_i}}{\tau_{\mathrm{off},i}}}, & t \ge \frac{p_i}{2f_i}. \end{cases} \tag{4}$$

Further, we have $c_i = \left(1 - e^{-p_i/(f_i \tau_{\mathrm{on},i})}\right)$ such that $h_i(t)$ a continuous function. When $\{\tau_{\mathrm{on},i}, \tau_{\mathrm{off},i}\} \ll p_i/f_i$, i.e., the pulsewidth is much larger than $\tau_{\mathrm{on},i}$ and $\tau_{\mathrm{on},i}$, we have $h_i(t) \approx \mathrm{rect}(t f_i/p_i)$.

B. Indoor Light Propagation

The LED light propagates through the indoor environment and reaches the sensor location possibly via multiple paths, as studied for instance in [12] and [13]. The multi-path effect, however, can be neglected because of the low frequency range, i.e., 2 to 4 kHz, considered in this paper and the large bandwidth, e.g., 10–50 MHz [14], of the free-space light propagation channel. Therefore, the optical signal at the sensor can be written as

$$x_{\mathrm{s}}(t) = \sum_{i=1}^{L} \alpha_i x_i(t) = \sum_{i=1}^{L} \sum_{n=-\infty}^{\infty} a_{\mathrm{I},i} h_i\left(t - t_i - n\frac{1}{f_i}\right) \tag{5}$$

where $a_{\mathrm{I},i} = \alpha_i a_{\mathrm{F},i}$ and α_i is the path loss of the free-space optical channel for the ith LED [6], [7].

C. Optical-Electrical Conversion

The photodiode in the sensor converts the optical signal $\alpha_i x_i(t)$ into an electrical signal $y_i(t)$. The responsitivity, ζ_i, for the ith LED is dependent on the color of the LED. The transient time of the photodiode is generally so small that the transient effect of the photodiode can be considered negligible [15], [16]. At the output of the photodiode, in response to each signal $\alpha_i x_i(t)$, we get

$$y_i(t) = \sum_{n=-\infty}^{\infty} a_i h_i \left(t - t_i - n\frac{1}{f_i} \right) \tag{6}$$

where $a_i = \zeta_i a_{\mathrm{I},i} = \zeta_i \alpha_i a_{\mathrm{F},i}$. The total output of the photodiode in response to all the LEDs can thus be written as $y_{\mathrm{s}}(t) = \sum_{i=1}^{L} y_i(t)$.

D. Channel Disturbances

There are mainly three types of channel disturbances, viz. disturbances from other light sources, electronics noise and shot noise. There might be other light sources in an indoor environment, such as the sun light and fluorescent lamps, that might result in disturbances denoted by y_{other}. The electronics noise and shot noise can be both approximated as additive white Gaussian noises (AWGN) [6], [7], [14]. Hence, the received electrical signal is given by

$$\begin{aligned} y(t) &= \sum_{i=1}^{L} y_i(t) + y_{\mathrm{other}} + v(t) \\ &= \sum_{i=1}^{L} \sum_{n=-\infty}^{\infty} a_i h_i \left(t - t_i - n\frac{1}{f_i} \right) + y_{\mathrm{other}} + v(t) \end{aligned} \tag{7}$$

where $v(t)$ denotes the noise term. The double-sided power spectrum density of $v(t)$ is denoted by $N_0/2$.

The light from other sources fluctuates at frequencies either much lower or much higher than the frequency range considered in this paper, i.e., 2 to 4 kHz. Therefore, y_{other} does not behave as a strong interference to the illumination sensing application. Moreover, for a practical indoor environment with an illuminance intensity of 1000 lux (lumen/m^2) and a photodiode with an area of 10 mm^2, N_0 is typically in the order of 10^{-24} ampere^2/Hz. The value of a_i, e.g., when a sensor lies in the center of a narrow LED beam, is, by contrast, in the order of 10^{-6} ampere. Therefore, the noise is almost negligible in practice. Now, the remaining challenge is to estimate a_i for each i from $y(t)$.

V. Sensor Processing

A. Estimation of a_i Based on the Fundamental Frequency Component

The main challenge for the sensor processing is to estimate a_i for each LED. In the FDM scheme, the illumination pulse trains from different LEDs are configured to have different fundamental frequencies f_i. This difference is reflected in the spectrum of $y_i(t)$, as derived in Appendix I,

$$Y_i(f) = \sum_{m=-\infty}^{\infty} a_i f_i H_i(mf_i) e^{-j2\pi m f_i t_i} \delta(f - mf_i) \tag{8}$$

where $\delta(\cdot)$ denotes the Kronecker delta function and $H_i(f)$ is the Fourier transform of $h_i(t)$, i.e., $H_i(f) = \int_{-\infty}^{\infty} h_i(t) \exp(-j2\pi ft) \mathrm{d}t$.

From (8), the spectrum of $y_i(t)$ consists of multiple lines at frequencies mf_i where $m = 0, \pm 1, \pm 2, \ldots$. In this paper, we present an approach that is based on the spectrum of $y(t)$ in the range of the fundamental frequencies between 2 and 4 kHz, i.e., we consider only $m = \pm 1$. In the following, we always implicitly assume a filter is applied such that only the signal band from 2 to 4 kHz remains in $y(t)$. The reasons for taking only this frequency range are fourfold. First, each f_i is distinct while there is potential overlap in the higher harmonics of f_i for different i. Second, we are, in principle, already able to estimate each a_i from the fundamental frequency component alone. For instance, from (8), the magnitude of $Y_i(f)$ at f_i is $|Y_i(f_i)| = a_i f_i H_i(f_i)$, hence we can take $\hat{a}_i = |Y_i(f_i)|/(f_i H_i(f_i))$. Third, another advantage is that the term $f_i H_i(f_i)$ can be shown as presented in Appendix II to be well approximated by $\sin(\pi p_i)/\pi$, irrespective of the precise ON- and OFF-switch characteristics of the LEDs. The magnitudes of higher frequency components are however in principle more dependent on the transient effects in $h(t)$, e.g., on τ_{on} and τ_{off}, which are not easy to be obtained accurately. Finally, there is no strong interference in this frequency range as explained in Section IV-D.

Therefore, in the following sections, we will focus on only the fundamental frequency components. The research challenge then turns out to be similar to that of amplitude estimation of multiple sinusoids. The problem of amplitude estimation, or in general parameter estimation, of multiple sinusoids was studied in literature, e.g., [17], for different applications. In this paper, in contrast, we focus on the application of illumination sensing and study the fundamental tradeoffs among the number of LEDs L, the response time T and allowable frequency inaccuracy in each f_i. Moreover, we apply a simple and yet efficient filter bank estimator in the sensor processing. The design of the filter response is also addressed to support as many LEDs as possible, and yet achieving an estimation performance that is robust against frequency inaccuracies.

B. Filter Bank Estimators

From (7), we need to estimate each a_i in the presence of the signals from other LEDs. It is known from the FDM scheme that the spectra of the signals from different LEDs are separated by a frequency spacing Δ_f, therefore, an intuitive approach is to try to separate the signals in the frequency domain and then perform the estimation.

We therefore consider applying a bank of bandpass filters to $y(t)$, followed by an envelope detector and a scaling operation. The block diagram is illustrated in Fig. 3. Here, for simplicity, we only show the ith branch of the filter bank. The impulse response of the ith bandpass filter is denoted by $g_i(t)$, corresponding to the ith LED. Without loss of generality, we assume $|G_i(f_i)| = 1$, where $G_i(f)$ is the Fourier transform of $g_i(t)$. Let T_g denote the *support* of $g_i(t)$, i.e., the time interval when $g_i(t) \neq 0$. In a practical application scenario, when a user gives the order of starting the estimation process, the estimator can give a stable output only after an interval T_g. Ideally, the filtered

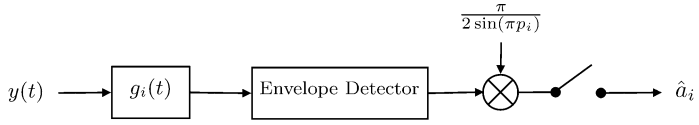

Fig. 3. Block diagram of the ith branch of a filter bank estimator.

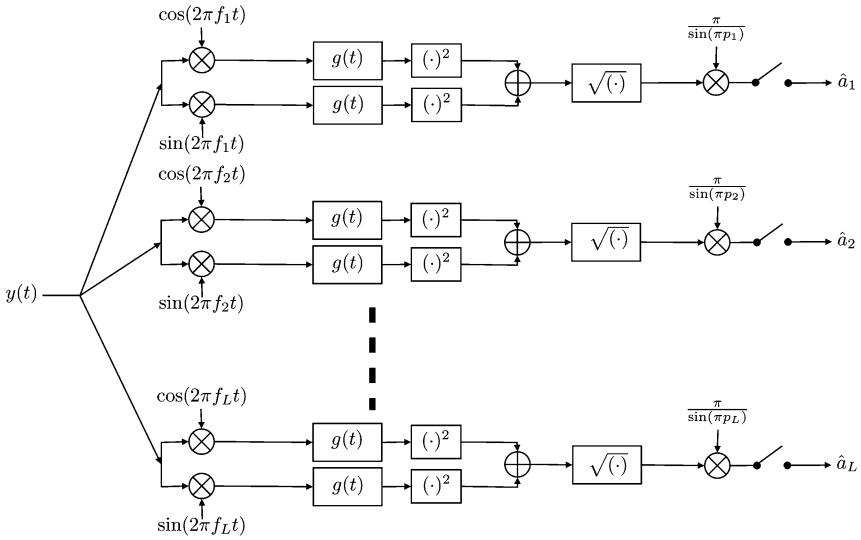

Fig. 4. Block diagram of the equivalent filter bank estimator approach.

signal $y(t) * g_i(t)$ then contains only a single sinusoid, therefore, the envelope detector gives a constant value that is ideally $2\sin(\pi p_i)a_i/\pi$. We can thus in principle sample the output of the envelope detector at any time t after the T_g interval to obtain an estimate $\hat{a}_i$. Due to the requirement on the response time T (see Section II), we need to have $T_g \leq T$. In the following, we will assume $T = T_g$, i.e., the support of $g_i(t)$ is $0 \leq t \leq T$.

Further, due to the uniform frequency spacing Δ_f between LEDs, it is sufficient to design the filters such that the responses $G_i(f)$ for different i are identical, except that the center frequencies are different. Equivalently, we can write $G_i(f) = G(f - f_i) + G^*(-f - f_i)$ for each i, where $G(f)$ is a low-pass filter and $|G(0)| = 1$. It is thus sufficient to design $G(f)$ for such filter bank estimator. Further, we assume $g(t)$, which is the inverse Fourier transform of $G(f)$, is a real-valued function, i.e., $G^*(f) = G(-f)$. Hence, we have $G_i(f) = G(f - f_i) + G(f + f_i)$, or equivalently, $g_i(t) = 2g(t)\cos(2\pi f_i t)$. The support of $g(t)$ is thus also $0 \leq t \leq T$. We obtain that $G(0)$ is also real-valued and thus $G(0) = \pm 1$. Without loss of generality, we will consider only the functions with $G(0) = 1$. The filtered signal is thus

$$\begin{aligned} &y(t) * g_i(t) \\ &\quad = \int_{-\infty}^{\infty} 2y(\phi)g(t-\phi)\cos(2\pi f_i t - 2\pi f_i \phi)\mathrm{d}\phi \\ &\quad = \cos(2\pi f_i t)\int_{t-T}^{t} 2y(\phi)\cos(2\pi f_i \phi)g(t-\phi)\mathrm{d}\phi \\ &\qquad + \sin(2\pi f_i t)\int_{t-T}^{t} 2y(\phi)\sin(2\pi f_i \phi)g(t-\phi)\mathrm{d}\phi. \quad (9) \end{aligned}$$

The envelope detector thus gives (10), shown at the bottom of the page. Hence, using (39), which is presented in Appendix II, we obtain an equivalent filter bank estimator

$$\hat{a}_i(t) = \frac{\pi}{\sin(\pi p_i)}\left|\int_{t-T}^{t} y(\phi)e^{j2\pi f_i \phi}g(t-\phi)\mathrm{d}\phi\right|. \quad (11)$$

The block diagram of this filter bank estimator is illustrated in Fig. 4.

Finally, from (11), we also have

$$\begin{aligned} \hat{a}_i(t) &= \frac{\pi}{\sin(\pi p_i)}\left|\int_{0}^{T} y(t-\phi)e^{j2\pi f_i (t-\phi)}g(\phi)\mathrm{d}\phi\right| \\ &= \frac{\pi}{\sin(\pi p_i)}\left|\int_{0}^{T} y(t-\phi)g(\phi)e^{-j2\pi f_i \phi}\mathrm{d}\phi\right|. \quad (12) \end{aligned}$$

This estimator is then equivalent to taking a block of data $y(t)$ from $t - T$ to t, applying a windowing function $g(t)$ and then taking the Fourier transform. A more efficient implementation

$$\sqrt{\left(\int_{t-T}^{t} 2y(\phi)\cos(2\pi f_i \phi)g(t-\phi)\mathrm{d}\phi\right)^2 + \left(\int_{t-T}^{t} 2y(\phi)\sin(2\pi f_i \phi)g(t-\phi)\mathrm{d}\phi\right)^2} = \left|\int_{t-T}^{t} 2y(\phi)e^{j2\pi f_i \phi}g(t-\phi)\mathrm{d}\phi\right|. \quad (10)$$

is thus via the fast Fourier transform (FFT), as we will detail in Section VII.

In the next section, due to the equivalence between (11) and (12), it is sufficient to only investigate the performance of the filter bank estimator described in (11) and shown in Fig. 4. We already see that the performance of the estimator is quite dependent on $g(t)$, especially on how well $g(t)$ can separate the signals from different LEDs given a small support T. Therefore, as a key issue, the design of $g(t)$ will also be discussed.

VI. Performance Evaluation and Design of the Filter Response

A. Ideal Case Without Frequency Offsets

In this section, we investigate the case when there are no frequency inaccuracies in any f_i. Then from (8), (11), and (39), which is presented in Appendix II, we get (13) and (14), shown at the bottom of the page, where $\psi_m = -j2\pi f_m t_m$, $\psi_i = -j2\pi f_i t_i$, and v_i is the noise term with variance $(N_0/2)\int_{-\infty}^{\infty} g^2(t)\mathrm{d}t$. Thus, the estimation error

$$|\hat{a}_i(t) - a_i| \le a_i|(G(0)-1)| + \sum_{m\neq i} a_m \frac{\sin(\pi p_m)}{\sin(\pi p_i)}|G((m-i)\Delta_f)| + |v_i|. \quad (15)$$

Then, we can perfectly separate the signals from different LEDs, and thus the optimum estimation performance can be achieved, if the following conditions on $G(f)$ are satisfied.

Condition (a): $G(0) = 1$;

Condition (b): $G(n\Delta_f) = 0$ for $n \neq 0$.

Condition (c): $g(t)$ is a real-valued function with support $0 \le t \le T$.

If these conditions are satisfied, we get from (1) that

$$\xi_i = 10\log\frac{|v_i|p_i}{\sum_m a_m p_m}. \quad (16)$$

From the numerical discussion in Section IV-D, we conclude that the estimation error is negligible. Hence, the system requirement on *accuracy of illumination sensing* is satisfied.

Further, from the first two conditions, we obtain that $G(f)$ is actually a Nyquist-1 function of f, satisfying the Nyquist pulse shaping criterion [18]. Therefore, we have

$$\sum_n g\left(t + n\frac{1}{\Delta_f}\right) = \Delta_f. \quad (17)$$

Thus the minimum support of $g(t)$ is $1/\Delta_f$, which is achieved by and only by setting $g(t)$ to be a rectangular function $g(t) = (1/T)\mathrm{rect}(t/T - 1/2)$. Hence, we have $T \ge 1/\Delta_f$ and $L = W/\Delta_f \le WT$. In other words, given the requirement on T, i.e., *high speed illumination sensing*, the maximum number of LEDs that can be supported is $L_{\max} = WT$. For instance, for $W = 2000$ kHz and $T = 0.1$ s, we have $L_{\max} = 200$.

B. Worst Cases With Frequency Offsets

As introduced in Section II, in practice, there is always some frequency inaccuracy in f_i. Due to the low cost design, the frequency inaccuracy can be as high as 100 ppm. Let f_i and $\bar{f}_i$ denote the actual and ideal fundamental frequency, respectively. The frequency offset, ϵ_i (in Hertz), is defined as $\epsilon_i \triangleq f_i - \bar{f}_i$. The estimation error can thus be obtained, similarly to (15), as

$$|\hat{a}_i(t) - a_i| \le a_i|(1 - |G(\epsilon_i)|)| + \sum_{m\neq i} a_m \frac{\sin(\pi p_m)}{\sin(\pi p_i)}|G((m-i)\Delta_f + \epsilon_m)| + |v_i|. \quad (18)$$

From (1), the cost function can be written as

$$\xi_i \le 10\log\left(\frac{a_i p_i}{\sum_{m=1}^{L} a_m p_m}(1 - |G(\epsilon_i)|) + \frac{\sum_{m\neq i} a_m p_i \frac{\sin(\pi p_m)}{\sin(\pi p_i)}|G((m-i)\Delta_f + \epsilon_m)|}{\sum_{m=1}^{L} a_m p_m}\right) \quad (19)$$

where noise is neglected. There are two terms in the log function. The first term is due to the frequency offset of the ith LED itself, and the second term is the impact of other LEDs on the estimation of a_i. For convenience, we name these two terms *bias error* and *interference*, and denote them by ξ_i^{b} and ξ_i^{i}, respectively.

Now, it can be seen that ξ_i is a function of $\{\epsilon_m\}, \{p_m\}, \{a_m\}$ where $m = 1, 2 \ldots L$, $G(f)$ and Δ_f. The range of $\{\epsilon_m\}$ is determined by the clock inaccuracies, while the specific values are unknown to the sensor. The parameters $\{p_m\}$ are determined by the lighting functionalities and each p_m can be anything between $p_{\min} = 0.001$ and $p_{\max} = 0.97307$ (see Section III). The range of $\{a_m\}$ is dependent on the physical channel characteristics (see Section IV), such as the free-space optical path loss. The value of optical path loss can be significantly different for different LEDs [6], [7], especially when considering the case when the sensor lies in the center of an LED beam, yet very far from the light beam of another LED. Hence, in order to design $G(f)$ and Δ_f such that the system requirements can be satisfied in all cases, we consider the worst case conditions for ξ_i to be maximum. For simplicity, we first consider the case with only two LEDs and later extend to more LEDs.

$$\hat{a}_i(t) = \frac{\left|\sum_{m=1}^{L} a_m \frac{1}{\pi}\sin(\pi p_m) e^{-j2\pi f_m t_m} e^{j2\pi(f_m - f_i)t} G(f_m - f_i) + v_i\right|}{\frac{1}{\pi}\sin(\pi p_i)} \quad (13)$$

$$= \left|a_i G(0) + \sum_{m\neq i} a_m \frac{\sin(\pi p_m)}{\sin(\pi p_i)} e^{j2\pi(m-i)\Delta_f t + \psi_m - \psi_i} G((m-i)\Delta_f) + v_i e^{-\psi_i}\right|, \quad (14)$$

1) Worst Case for $L = 2$: Assume there are two LEDs, namely LED_1 and LED_2. Here, we focus on ξ_1, and the results for ξ_2 can be obtained similarly. From (19), we get

$$\xi_1^{\mathrm{b}} = \frac{1}{1+\frac{a_2 p_2}{a_1 p_1}}(1-|G(\epsilon_1)|) \tag{20}$$

$$\xi_1^{\mathrm{i}} = \frac{1}{\frac{a_1}{a_2}+\frac{p_2}{p_1}}\frac{\sin(\pi p_2)}{\sin(\pi p_1)}|G(\Delta_f+\epsilon_2)|. \tag{21}$$

The worst case condition for the ξ_1^{b} can be seen to be $a_1 p_1 \gg a_2 p_2$, i.e., when the illuminance from LED_1 is much larger than that from LED_2. With respect to the *interference* ξ_1^{i}, we can see that the interference term keeps increasing while a_1/a_2 decreases, and converges to a certain value when $a_1/a_2 \ll p_2/p_1$, or equivalently $a_1 p_1 \ll a_2 p_2$. This condition corresponds to the case when the illuminance from LED_1 is much smaller than that from LED_2. Then the interference is proportional to $\mathrm{sinc}(\pi p_2)/\mathrm{sinc}(\pi p_1)$. Hence, the worst case is when $p_2 \to 0$ and $p_1 \to 1$. From the discussion in Section III, we can take $p_2 = p_{\min} = 0.001$ and $p_1 = p_{\max} = 0.97307$. From the above investigation on the worst case, we have

$$\xi_1^{\mathrm{b}} \le 1-|G(\epsilon_1)| \tag{22}$$

$$\xi_1^{\mathrm{i}} \le \frac{\mathrm{sinc}(\pi p_{\min})}{\mathrm{sinc}(\pi p_{\max})}|G(\Delta_f+\epsilon_2)| = 36.2|G(\Delta_f+\epsilon_2)|. \tag{23}$$

Note that ξ_1^{b} and ξ_1^{i} do not approach their upper bounds simultaneously. In fact, when ξ_1^{i} approaches its upper bound, i.e., $a_1 p_1 \ll a_2 p_2$, ξ_1^{b} approaches zero. We will later evaluate these two terms separately.

2) Worst Case for $L > 2$: When there are more than two LEDs, without loss of generality, we still focus on the first LED, then we have

$$\xi_1^{\mathrm{b}} = \frac{1}{1+\frac{\sum_{m=2}^{L} a_m p_m}{a_1 p_1}}(1-|G(\epsilon_1)|) \le 1-|G(\epsilon_1)| \tag{24}$$

$$\xi_1^{\mathrm{i}} = \frac{1}{\pi \mathrm{sinc}(\pi p_1)} \times \frac{\sum_{m=2}^{L} a_m \sin(\pi p_m)|G((m-1)\Delta_f+\epsilon_m)|}{\sum_{m=1}^{L} a_m p_m} \tag{25}$$

where we can approach the upper bound on ξ_1^{b} when $\sum_{m=2}^{L} a_m p_m \ll a_1 p_1$, i.e., the total illuminance from all the other LEDs is much smaller than that from LED_1. The bound on ξ_1^{i} can be obtained as follows. First, when the frequency spacing between the mth LED and the first LED is larger, it is in principle easier to separate the frequency components. Therefore, the interference term is upper bounded by the case when the spacing between any f_m where $m \ge 2$ and f_1 is Δ_f, i.e., the spacing between two closest frequencies. Moreover, when $\sum_{m=2}^{L} a_m p_m \gg a_1 p_1$, we approach an upper bound on ξ_1^{i}

$$\xi_1^{\mathrm{i}} \le \frac{|G(\Delta_f+\epsilon_2)|}{\mathrm{sinc}(\pi p_1)}\frac{\sum_{m=2}^{L} a_m \sin(\pi p_m)}{\sum_{m=2}^{L} a_m \pi p_m} \le \frac{|G(\Delta_f+\epsilon_2)|}{\mathrm{sinc}(\pi p_{\max})}\frac{\sum_{m=2}^{L} a_m \sin(\pi p_m)}{\sum_{m=2}^{L} a_m \pi p_m}. \tag{26}$$

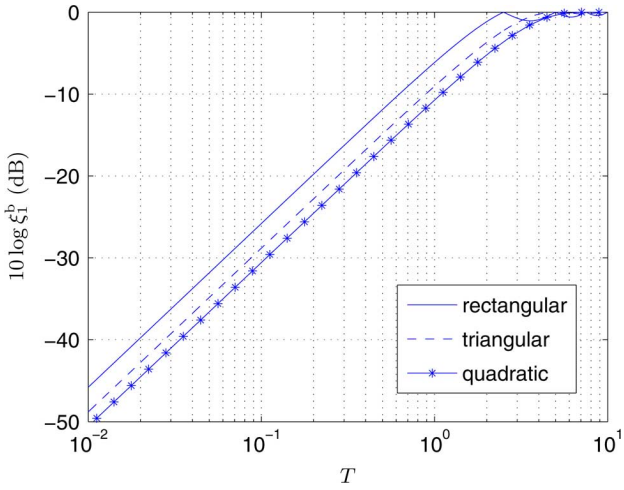

Fig. 5. Upper bound on the bias error ξ_1^{b} versus response time T at 100 ppm clock inaccuracy.

Further, we know that $\mathrm{sinc}(\pi p_m) = \sin(\pi p_m)/(\pi p_m)$ is monotonically decreasing with the increase of p_m when $0 \le p_m \le 1$, i.e., $\sin(\pi p_m)/(\pi p_m) \le \mathrm{sinc}(\pi p_{\min})$. Hence,

$$\frac{\sum_{m=2}^{L} a_m \sin(\pi p_m)}{\sum_{m=2}^{L} a_m \pi p_m} \le \frac{\sum_{m=2}^{L} a_m \pi p_m \mathrm{sinc}(\pi p_{\min})}{\sum_{m=2}^{L} a_m \pi p_m} = \mathrm{sinc}(\pi p_{\min}) \tag{27}$$

where the equality is achieved if $p_m = p_{\min}$ for every $2 \le m \le L$. We thus also have

$$\xi_1^{\mathrm{i}} \le \frac{\mathrm{sinc}(\pi p_{\min})}{\mathrm{sinc}(\pi p_{\max})}|G(\Delta_f+\epsilon_2)|. \tag{28}$$

Then in the worst case for $L > 2$, all the LEDs, except the first LED, have the identical frequency and duty cycle, thus this case is equivalent to the case with only two LEDs in the system. The worst case results in (24) and (28) are also identical to those in (22) and (23). It is therefore sufficient to only focus on the worst case for two LEDs when dealing with numerical results in the following sections.

3) Performance of the Rectangular Filter $g(t)$: Now, we evaluate the impact of the frequency offsets on the estimation performance. We consider the rectangular function introduced in Section VI-A, $g(t) = (1/T)\mathrm{rect}(t/T - 1/2)$, and thus $|G(f)| = |\mathrm{sinc}(\pi T f)|$. Given 100 ppm clock inaccuracy, we only need to consider $\{\epsilon_1, \epsilon_2\} = \pm 0.4$ Hz for the worst case scenario. The upper bound on ξ_1^{b} is thus $1-\mathrm{sinc}(0.4\pi T)$, which can be evaluated at different T, for which the numerical values are shown in Fig. 5. From Section II, we require $\xi_1 \le -20$ dB, i.e., $\xi_1^{\mathrm{b}} + \xi_1^{\mathrm{i}} \le 10^{-2}$. Fig. 5 shows that ξ_1^{b}, even in the worst case, is well below 10^{-2}, or $10\log\xi_1^{\mathrm{b}}$ is well below -20 dB, in the range of T of interest to us, i.e., $T \le 0.1$ second. It is therefore more important to consider ξ_1^{i} to be also below 10^{-2} in the worst case. In the following, we thus assume that ξ_1^{b} is negligible, so that

$$\xi_1 \approx 10\log_{10}(\xi_1^{\mathrm{i}}) = 10\log_{10}\frac{\mathrm{sinc}(\pi p_{\min})}{\mathrm{sinc}(\pi p_{\max})} + 10\log_{10}\max_{\epsilon_2=\pm 0.4}|\mathrm{sinc}(T\pi(\Delta_f+\epsilon_2))|. \tag{29}$$

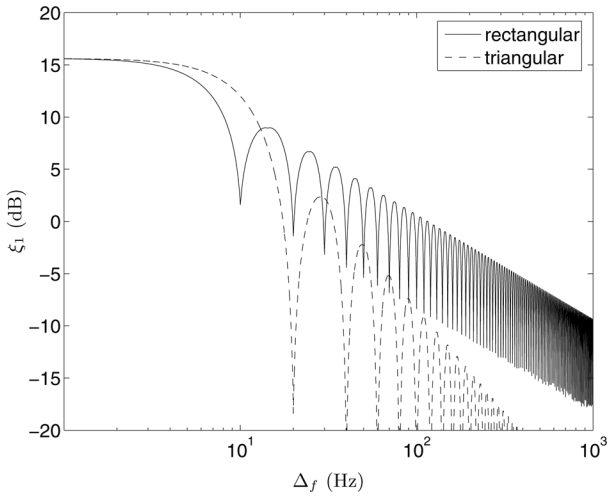

Fig. 6. Worst case ξ_1 with respect to the frequency spacing, at $T = 0.1$ s and 100 ppm clock inaccuracy.

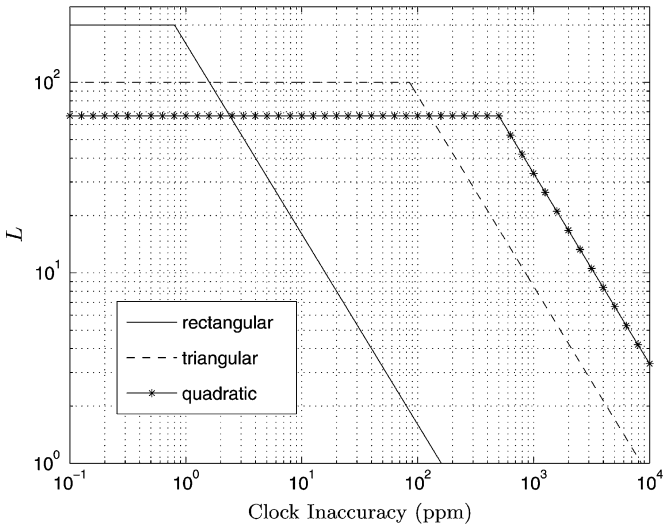

Fig. 7. Tradeoff between L and clock inaccuracy with $T \leq 0.1$.

The value of ξ_1 at $T = 0.1$ as a function of Δ_f is plotted in Fig. 6. Since $L = W/\Delta_f$, it can be observed that the use of a rectangular function $g(t)$ can not even support $\Delta_f = 1000$ Hz, and thus only a single LED can be accommodated with $W = 2$ kHz. Considering the fact that at most 200 LEDs can be accommodated in the ideal case without frequency offsets, we can conclude that the frequency inaccuracy plays a quite significant role in the estimation performance in terms of the maximum number of LEDs that can be supported.

Now, we investigate the tradeoff between L and the clock inaccuracies. From (29), while maintaining $T\Delta_f = 1$, the value of ξ_1 is only a function of $T \cdot \max_{\epsilon_2} |\epsilon_2|$. Based on this observation, we can obtain the tradeoff as follows. A very small clock inaccuracy, we know that $L = WT$ LEDs can be supported. Then, with a larger clock inaccuracy, i.e., a larger ϵ_2 in (29), the estimation error in terms of ξ_1 will also increase. There is a boundary value for the clock inaccuracy when the requirement $\xi_1 \leq -20$ dB will no longer be satisfied. Therefore, if the practical clock inaccuracy is larger than the boundary value, we have to reduce T proportionally such that $T \cdot \max_{\epsilon_2} |\epsilon_2|$ does not increase. Thus, $\Delta_f = 1/T$ has to be in turn increased. Equivalently, $L = W/\Delta_f = WT$ is decreased. The boundary value for the clock inaccuracy can be obtained easily through numerical evaluation. For instance, we can find that the boundary value is only 0.8 ppm to satisfy $\xi_1 \leq -20$ dB and $T \leq 0.1$ s. Therefore, we can obtain the tradeoff between the clock inaccuracy and L, as shown in Fig. 7. Note that L is upper bounded by $0.1W = 200$ because of $T \leq 0.1$ s. If this constraint on T can be relaxed, we can potentially support a larger L, provided that the clock inaccuracy is reduced, as will be discussed later in Section VI-D.

So far, we have investigated the tradeoff between L and the clock inaccuracy under the condition $T\Delta_f = 1$. Effectively, we focus on the first zero of the function $G(\Delta_f) = \mathrm{sinc}(\pi T \Delta_f)$. One can of course also investigate this tradeoff under $T\Delta_f = n$, where $n \geq 2$, i.e., corresponding to the nth zero of $G(\Delta_f)$. Through numerical evaluations, although not explicitly shown here, we observe that considering other zeros of $G(\Delta_f)$ does not result in a better tradeoff between L and the clock inaccuracy. We will thus only consider $\Delta_f = 1/T$ Hz for the rectangular function. Similarly, we will also only focus on the first zero of other considered $G(\Delta_f)$ in future sections.

From the tradeoff between L and clock inaccuracy shown in Fig. 7, the illumination sensing performance is quite limited through the use of the rectangular function, in the presence of frequency offsets. Therefore, in the following, we consider design of $g(t)$ such that the estimation performance is more robust against the frequency offsets.

C. Design of $g(t)$ in the Presence of Frequency Offsets

1) Triangular Function: In order to design $g(t)$ such that the estimation performance is robust against frequency offsets, we need to minimize $|1 - |G(\epsilon_1)||$ and $|G((m-1)\Delta_f + \epsilon_m)|$, (see (19)). Through the first-order Taylor expansion, we get

$$G(\epsilon_1) = 1 + G'(0)\epsilon_1 + O(\epsilon_1^2) \tag{30}$$

$$G((m-1)\Delta_f + \epsilon_m) = G'((m-1)\Delta_f)\epsilon_m + O(\epsilon_m^2) \tag{31}$$

where $G'(f)$ denotes the derivative of $G(f)$. Therefore, in order to obtain a lower $\max_{\epsilon_1} ||G(\epsilon_1)| - 1|$ and $\max_{\epsilon_m} |G((m-1)\Delta_f + \epsilon_m)|$, we can impose an additional constraint on the design of $g(t)$, i.e.,

Condition (d): $|G'(n\Delta_f)| = 0$, for any integer n.

Effectively, $G(f)$ is now a Nyquist-1 function with the additional *Condition* (d). We can thus consider the family of Nyquist-1 functions that can be written as $G(f) = G_1(f)G_2(f)$, where $G_1(f)$ is a Nyquist-1 function, which in general does not satisfy *Condition* (d), and $G_2(f)$ is an arbitrary function that is differentiable at $n\Delta_f$ and $G_2(0) = G(0)/G_1(0) = 1$. We then have

$$\begin{aligned} G'(n\Delta_f) &= G_1(n\Delta_f)G_2'(n\Delta_f) + G_1'(n\Delta_f)G_2(n\Delta_f) \\ &= G_1'(n\Delta_f)G_2(n\Delta_f). \end{aligned} \tag{32}$$

For $n \neq 0$, we can get that *Condition* (d) is satisfied if and only if $G_2(n\Delta_f) = 0$. Thus, $G_2(f)$ is also a Nyquist-1 function.

Hence, we get $g(t) = g_1(t) * g_2(t)$, where $*$ denotes the convolution operation. The support of $g(t)$ is therefore the sum of that of $g_1(t)$ and $g_2(t)$. The minimal support of $g(t)$ is thus $2/\Delta_f$, which is achieved when both $g_1(t)$ and $g_2(t)$ are rectangular functions, i.e., $g(t)$ is a triangular function. More specifically, $g(t) = (2/T)\text{rect}(2t/T - 1/2) * (2/T)\text{rect}(2t/T - 1/2)$ and can be written explicitly as

$$g(t) = \begin{cases} \frac{4}{T^2}t, & 0 \le t \le \frac{T}{2} \\ -\frac{4}{T^2}t + \frac{4}{T}, & \frac{T}{2} \le t \le T \\ 0, & \text{elsewhere.} \end{cases} \tag{33}$$

We can also obtain that

$$|G(f)| = \text{sinc}^2\left(\frac{1}{2}T\pi f\right). \tag{34}$$

It can be confirmed that this $g(t)$ also satisfies $G'(0) = 0$. Hence, *Condition* (d) is satisfied at any n. Note that the design of Nyquist-1 functions with a similar requirement was also investigated in other application contexts and under different optimization criteria [19]–[21]. To the best of our knowledge, we are the first to give the constraint condition in the form of *Condition* (d) and show that the triangular function has the minimum support, which is a desirable property for the illumination sensing application considered in this paper.

Moreover, since the filter bank estimator in (11) and that in (12) are equivalent, one might also consider some other functions from the widely used windowing functions, e.g., the Hann windowing function. These windowing functions are normally optimized to have low side lobes in $G(f)$. In our application, however, with the knowledge of ideal Δ_f and due to the fact that (ϵ_i/Δ_f) is quite small, we only need to focus on the zeros of the $G(\Delta_f)$ such that the performance is more robust against frequency offsets. Therefore, in this context, the triangular windowing function achieves better performance than all the windowing functions that are known to us. There are also a class of windowing functions called "flat-top" functions, where the mainlobe is flattened around the zero frequency. This "flat-top" property is desirable for the reduction of ξ_1^b, as defined in (20). To this end, we take this property into consideration in the *Condition* (d), which is presented earlier in this section, in particular for the case $n = 0$. Further, from the numerical results for the rectangular and triangular functions presented in Fig. 5, the bias error can be neglected. In fact, also from Fig. 5, the use of the triangular function further reduces ξ_1^{b} than that for the rectangular function. In view of above discussion, we thus do not consider the further optimization of the mainlobe behavior in this paper.

For the triangular function, the cost function ξ_1 in the worst case can thus be written as

$$\begin{aligned} \xi_1 &\approx 10\log_{10}(\xi_1^{\text{i}}) \\ &= 10\log_{10}\frac{\text{sinc}(\pi p_{\min})}{\text{sinc}(\pi p_{\max})} \\ &\quad + 10\log_{10}\max_{\epsilon_2=\pm 0.4}\left|\text{sinc}^2\left(\frac{1}{2}T\pi(\Delta_f + \epsilon_2)\right)\right| \end{aligned} \tag{35}$$

the numerical values of which are also plotted in Fig. 6. It can then be seen that there is significant improvement of the estimation performance, compared to the use of the rectangular function at $\Delta_f = 20$ Hz.

From above discussion on the minimum support, we have $2/\Delta_f \le T$. We thus also have $L = W/\Delta_f \le 1/2WT$, i.e., $L \le 100$ for $T = 0.1$ s and $W = 2$ kHz. Compared to the rectangular function, the use of the triangular function increases the robustness of the estimation performance against frequency offsets, while reducing the maximum number of LEDs that can be supported in the ideal case, i.e., the case without frequency offsets. Furthermore, similarly to the rectangular function, we may also investigate the tradeoff between L and a higher clock inaccuracy under the condition $\xi_1 \le -20$ dB and $T\Delta_f/2 = 1$, and the result is shown in Fig. 7. Note that L is always less than 100 for the triangular function because of the constraint $T \le 0.1$ s. It can be seen that the use of the triangular function can support significantly more LEDs than that of the rectangular function at a realistic clock inaccuracy, e.g., larger than 2 ppm. In particular, at 100 ppm clock inaccuracy, 85 LEDs can be accommodated by the use of the triangular function.

2) Higher Order Convolution of Rectangular Functions: We can further extend the triangular function by taking $g(t)$ to be even higher order convolution of rectangular functions. For instance, a third-order convolution results into $g(t) = (3/T)\text{rect}(3t/T - 1/2) * (3/T)\text{rect}(3t/T - 1/2) * (3/T)\text{rect}(3t/T - 1/2)$ and thus $|G(f)| = |\text{sinc}^3(1/3T\pi f)|$. For convenience, we name this $g(t)$ *piecewise quadratic function*, or even simply *quadratic function*. For this $g(t)$, we have $L \le WT/3$, and thus $L \le 66$ for $T \le 0.1$ s and $W = 2$ kHz. From Fig. 5, the bias error is also negligible. Further, through numerical investigation, we see that we can support 66 LEDs even at 500 ppm clock inaccuracy. Similarly to the rectangular and triangular function, we can also investigate the tradeoff between the clock inaccuracy and L for the piecewise quadratic function, and the numerical results are also shown in Fig. 7. From the results, it can be seen that the piecewise quadratic function outperforms the triangular function only when the clock inaccuracy is larger than 130 ppm. From above, it is also straightforward to further extend the results into fourth or even higher order of convolution of rectangular functions. However, since we focus on a realistic range of clock inaccuracy, e.g., at 100 ppm, the discussion on those functions is beyond the scope of this paper.

D. Tradeoff Between T and L

In the above, we discussed the design of $g(t)$ in order to maintain robustness against frequency offsets. In particular, we investigated the tradeoff between L and the clock inaccuracies under the constraint $T \le 0.1$ s. In this section, we study the illumination sensing performance with respect to the estimation time T. We believe that this study is of high practical value because a user is in principle able to have an accurate control of the estimation time T and that the requirement on T might be relaxed in certain application scenarios. In particular, we focus on the tradeoff between L and T in this section, provided that the condition on $\xi_i \le -20$ dB is always satisfied.

We focus on the performance for the triangular function. The tradeoff between L and T in this case can be obtained in two

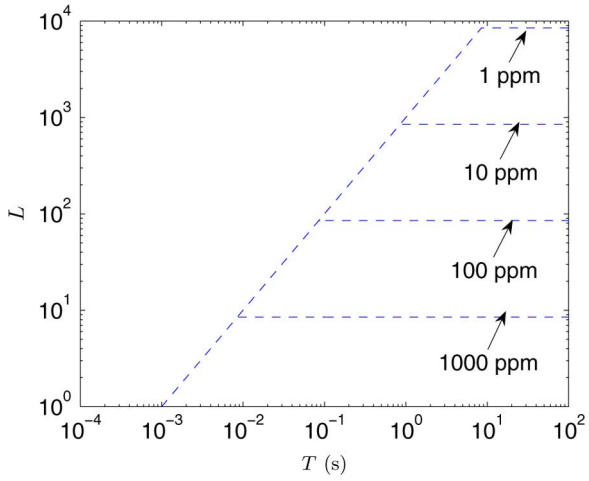

Fig. 8. Number of LEDs L versus response time T for the triangular function at different clock inaccuracies.

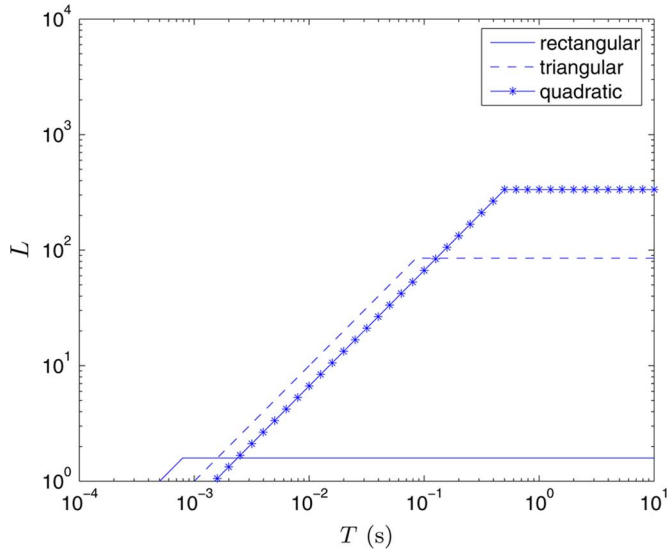

Fig. 9. Number of LEDs L versus response time T for different functions at 100 ppm clock inaccuracy.

steps. First, when T increases from zero, L is linearly proportional to T by $L = WT/2$. Second, the increase of T will result in a higher ξ_1 at given clock inaccuracy from (35). When T is increased above a certain value, the requirement on accurate illumination sensing will no longer be satisfied. Therefore, further increasing T beyond this value cannot result in a larger L. This boundary value for T can be obtained for the case of 100 ppm as follows. From Section VI-C-1) and as shown in Fig. 7, at most 85 LEDs can be supported at 100 ppm, which corresponds to $T = 85/(W/2) = 0.085$ s. Thus, in practice, we would maintain $T = 0.085$ s even if we are allowed to have a larger T. The tradeoff between T and L for the triangular function at 100 ppm can thus be obtained as depicted in Fig. 8.

For a different clock inaccuracy, we can similarly obtain the tradeoff between L and T. The difference is that the range of T when we can have $L = WT/2$ is inversely-proportional to the clock inaccuracy, as indicated by (35). For instance, for 10 ppm clock inaccuracy, we can have $L = WT/2$ up to $T = (100/10) \times 0.085 = 0.85$ s. The tradeoff between T and L for different clock inaccuracies can thus be obtained as shown in Fig. 8. We can see that in order to accommodate more LEDs, we need to increase T and reduce the clock inaccuracy as well. For instance, if 1000 LEDs need to be accommodated, we should have a response time $T > 1$ s and a clock inaccuracy less than 10 ppm.

We can, of course, also obtain the tradeoffs for other possible functions $g(t)$ in the presence of different clock inaccuracies. The results for different $g(t)$ at 100 ppm are shown in Fig. 9. It can also be concluded from this figure that the use of the triangular function can accommodate more LEDs than other functions in the range $T \leq 0.1$ s. If the requirement on T is relaxed, however, e.g., when T can be larger than 0.1 s, the piecewise quadratic function can outperform the triangular function.

VII. Low-Cost Implementations

Here, we briefly remark on the implementation of the illumination sensing scheme shown in Fig. 4. In practice, such filter bank structure can be implemented in a high efficiency [22]. Moreover, since the triangular function is the convolution of two rectangular functions, the filter with the triangular impulse response can be simply implemented by a concatenation of two sliding-window integrators, with the integration time of each integrator to be $T/2$. For a low-cost implementation of such sliding-window integrators, we can use digital circuits instead of analog ones. This implementation can be extended to piecewise quadratic functions by simply adding one more sliding-window integrator. Further, we can shift the sampler in Fig. 4 forward such that the sampler is located immediately after the $G(f)$ block. Thus, we only need to perform the operations following the $G(f)$ block, such as the squaring block, once per sample.

Another different implementation is through the use of (12). We can first sample $y(t)$, and in turn apply the windowing function $g(t)$ in the discrete-time domain. Finally, we perform fast Fourier transform (FFT), which can be implemented at a high efficiency, to obtain the spectra at desired frequencies simultaneously. Subsequently, we can normalize the magnitude of the spectrum at each frequency f_i to obtain $\hat{a}_i$, i.e., $\hat{a}_i = (\pi/\sin(\pi p_i))|Y(f_i)|$. Fig. 10 illustrates this low complexity implementation of the block diagram in Fig. 4. In Fig. 10, $y[n]$ denotes the discrete-time samples of $y(t)$, $\mathbf{y}$ denotes a vector of samples $y[n]$, $\mathbf{y}_w$ denotes the windowed version of $\mathbf{y}$. Due to the Nyquist sampling theorem, the sampling frequency for $y(t)$ is at least $2W$. The support of $g(t)$ is $2/\Delta_f = 2/(W/L) = 2L/W$. Hence, a window of $2W \times (2L/W) = 4L$ samples is needed, and an FFT operation with the size $4L$ is thus sufficient. More detailed discussion on other practical implementation issues, such as the suppression of out-of-the-band noise, and quantization resolution of the analog-to-digital conversion, is beyond the scope of this paper.

VIII. Conclusion

In this paper, the key challenges of illumination sensing in LED lighting systems are described and investigated. A simple FDM scheme is investigated to facilitate simultaneous estimation of the illuminance of a large number of LEDs. We present three filter bank sensor structures that are based on equivalent

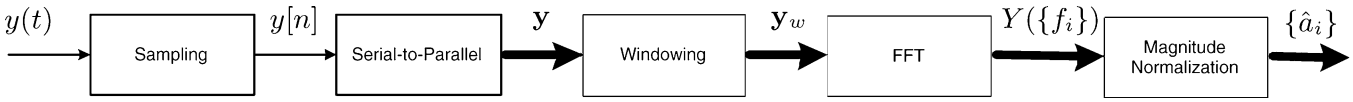

Fig. 10. Low-complexity implementation of the filter bank estimator.

principles, although with different implementations. The design of filter responses, in the context of supporting maximum number of LEDs while satisfying other estimation requirements such as high speed and accurate illumination sensing, is also discussed. It is shown that the rectangular function can support the maximum number of LEDs for the ideal case without frequency inaccuracies. When considering frequency inaccuracies in a practical range, the optimum filter response involves multiple convolutions of rectangular functions. In particular, the triangular function, which is the convolution of two rectangular functions, gives a better tradeoff, than all the other considered functions, between the number of LEDs that can be supported and the clock inaccuracies within a practical range of interest. More specifically, 85 LEDs can be supported for a response time of 0.1 s and 100 ppm clock inaccuracy. We also show that the use of a piecewise quadratic function can give better performance than the triangular function when the clock inaccuracy is more than 130 ppm. Finally, the sensor structure proposed in this paper can be implemented at a very low cost. Hence, we conclude that a large number of LEDs can be accommodated with a simple FDM scheme and a low-cost filter-bank based sensor structure for the purpose of illumination sensing.

Appendix I
Derivation of (8)

Let $\mathcal{F}[\cdot]$ denote the operation of Fourier transform, we have $\mathcal{F}[h_i(t)] \triangleq H_i(f) = \int_{-\infty}^{\infty} h_i(t)e^{-j2\pi ft}\mathrm{d}t$, and thus

$$\begin{aligned}\mathcal{F}[h_i(t-t_i)] &= \int_{-\infty}^{\infty} h_i(t-t_i)e^{-j2\pi ft}\mathrm{d}t \\ &= H_i(f)e^{-j2\pi ft_i}. \end{aligned} \tag{36}$$

Moreover, From [23], for any function $z(t)$ whose Fourier transform exists and is denoted by $Z(f)$, we have

$$\mathcal{F}\left[\sum_{n=-\infty}^{\infty} z(t-n/f_i)\right] = \sum_{m=-\infty}^{\infty} f_i Z(mf_i)\delta(f-mf_i). \tag{37}$$

Now, letting $z(t) = h_i(t-t_i)$, we can substitute $Z(f) = H_i(f)e^{-j2\pi ft_i}$ into (37) and obtain

$$\begin{aligned}&\mathcal{F}\left[\sum_{n=-\infty}^{\infty} h_i(t-t_i-n/f_i)\right] \\ &\quad = \sum_{m=-\infty}^{\infty} f_i H_i(mf_i)e^{-j2\pi mf_i t_i}\delta(f-mf_i). \end{aligned} \tag{38}$$

Finally, from (6) and (38), we can obtain (8).

Appendix II
Evaluation of $f_iH_i(f_i)$

Here, we assume $1/f_i \gg \tau_{\mathrm{on}}$ and $1/f_i \gg \tau_{\mathrm{off}}$. When p_i is large, we have $p_i/f_i \gg \tau_{\mathrm{on}}$ and $p_i/f_i \gg \tau_{\mathrm{off}}$, $h_i(t)$ in (4) is approximately rectangular, i.e., $h_i(t) \approx \mathrm{rect}(tf_i/p_i)$. Thus, we have $f_iH_i(f_i) \approx \sin(\pi p_i)/\pi$.

Then, when p_i is very small and p_i/f_i is comparable to τ_{on} and τ_{off}, it can be obtained from (4) that

$$\begin{aligned} f_iH_i(f_i) &= \frac{1}{\pi}\sin(\pi p_i) - e^{j\pi p_i}\frac{1-e^{-\frac{p_i}{f_i\tau_{\mathrm{on}}}-j2\pi p_i}}{\frac{1}{f_i\tau_{\mathrm{on}}}+j2\pi} \\ &\quad + e^{-j\pi p_i}\left(1-e^{-\frac{p_i}{f_i\tau_{\mathrm{on}}}}\right)\frac{1}{\frac{1}{f_i\tau_{\mathrm{off}}}+j2\pi} \\ &\approx \frac{1}{\pi}\sin(\pi p_i) - \left(1-e^{-\frac{p_i}{f_i\tau_{\mathrm{on}}}}\right) \\ &\quad \times\left(\frac{1}{\frac{1}{f_i\tau_{\mathrm{on}}}+j2\pi}-\frac{1}{\frac{1}{f_i\tau_{\mathrm{off}}}+j2\pi}\right) \\ &\approx \frac{1}{\pi}\sin(\pi p_i) - \left(1-e^{-\frac{p_i}{f_i\tau_{\mathrm{on}}}}\right)f_i(\tau_{\mathrm{on}}-\tau_{\mathrm{off}}) \\ &\approx \frac{1}{\pi}\sin(\pi p_i) \end{aligned} \tag{39}$$

where the first approximation follows from $e^{j\pi p_i} \approx 1$ and $e^{j2\pi p_i} \approx 1$ because of $p_i \approx 0$, and the second approximation follows from $1/f_i \gg \tau_{\mathrm{on}}$ and $1/f_i \gg \tau_{\mathrm{off}}$. Finally the last approximation is because of $1/f_i \gg \tau_{\mathrm{on}} - \tau_{\mathrm{off}}$.

Acknowledgment

The authors would like to acknowledge valuable discussions with J.-P. Linnartz, J. Talstra, A. Pandharipande, and L. Feri. The authors would also like to thank the anonymous reviewers for their valuable comments and suggestions.

References

[1] S. Muthu, F. J. P. Schuurmans, and M. D. Pashley, "Red, green, and blue LEDs for white light illumination," *IEEE J. Sel. Topics Quantum Electron.*, vol. 8, no. 2, pp. 333–338, Mar./Apr. 2002.
[2] G. Pang, T. Kwan, H. Liu, and C.-H. Chan, "LED wireless," *IEEE Ind. Appl. Mag.*, vol. 8, no. 1, pp. 21–28, Jan./Feb. 2002.
[3] Lumileds. [Online]. Available: http://www.lumileds.com/products/
[4] Luxeon Star LEDs. [Online]. Available: http://www.luxeonstar.com/faqs.php
[5] *Digital Addressable Lighting Interfaces*, IEC 62386, 2007.
[6] J.-P. M. G. Linnartz, L. Feri, H. Yang, S. B. Colak, and T. C. W. Schenk, "Communications and sensing of illumination contributions in a power LED lighting system," in *Proc. IEEE Int. Conf. Communications (ICC)*, May 2008, pp. 5396–5400.
[7] J.-P. M. G. Linnartz, L. Feri, H. Yang, S. B. Colak, and T. C. W. Schenk, "Code division-based sensing of illumination contributions in solid-state lighting systems," *IEEE Trans. Signal Process.*, vol. 57, no. 10, pp. 3984–3998, Oct. 2009.
[8] M. Salsbury and I. Ashdown, "Adapting radio technology to LED feedback systems," in *Proc. SPIE*, 2007, vol. 6669.
[9] T. Komine and M. Nakagawa, "Fundamental analysis for visible-light communication system using LED lights," *IEEE Trans. Consum. Electron.*, vol. 50, no. 1, pp. 100–107, Feb. 2004.
[10] P. R. Boyce, *Human Factors in Lighting*, 2nd ed. Boca Raton, FL: CRC, 2003.

[11] A. Descombes and W. Guggenbiihl, "Large signal circuit model for LED's used in optical communication," *IEEE Trans. Electron. Devices*, vol. ED-28, no. 4, pp. 395–404, Apr. 1981.
[12] F. R. Gfeller and U. Bapst, "Wireless in-house communication via diffuse infrared radiation," *Proc. IEEE*, vol. 67, no. 11, pp. 1474–1486, Nov. 1979.
[13] J. M. Kahn and J. R. Barry, "Wireless infrared communications," *Proc. IEEE*, vol. 85, no. 2, pp. 265–298, Feb. 1997.
[14] J. R. Barry, *Wireless Infrared Communications*. Boston, MA: Kluwer, 1994.
[15] D. Wood, *Optoelectronic Semiconductor Devices*. Englewood Cliffs, NJ: Prentice-Hall, 1994, ch. 1–3, 5, 6.
[16] A. E. Iverson and D. L. Smith, "Mathematical modeling of photoconductor transient response," *IEEE Trans. Electron. Devices*, vol. 34, pp. 2098–2107, Oct. 1987.
[17] P. Stoica and R. L. Moses, *Spectral Analysis of Signals*. Englewood Cliffs, NJ: Prentice-Hall, 2005.
[18] J. G. Proakis, *Digital Communications*. New York: McGraw-Hill, 2000.
[19] L. E. Franks, "Further results on Nyquist's problem in pulse transmission," *IEEE Trans. Commun. Technol.*, vol. 16, pp. 337–340, 1968.
[20] J. Q. Scanlan, "Pulses satisfying the Nyquist criterion," *Electron. Lett.*, vol. 28, pp. 50–52, 1992.
[21] N. C. Beaulieu and M. O. Damen, "Parametric construction of Nyquist-I pulses," *IEEE Trans. Commun.*, vol. 52, pp. 2134–2142, 2004.
[22] P. P. Vaidyanathan, *Multirate Systems and Filter Banks*. Englewood Cliffs, NJ: Prentice-Hall, 1992.
[23] A. V. Oppenheim, R. W. Schafer, and J. R. Buck, *Discrete-Time Signal Processing*. Englewood Cliffs, NJ: Prentice-Hall, 1999, ch. 4.

Hongming Yang (S'06–M'09) received the B.S. and M.S. degrees from the Department of Electronic Engineering, Tsinghua University, Beijing, China, in 2000 and 2003, respectively. He also received the M.E. degree from the Department of Electrical and Computer Engineering, National University of Singapore, Singapore, in 2005. He is now working towards the Ph.D. degree with Eindhoven University of Technology (TU/e), Eindhoven, The Netherlands, while conducting joint research with Philips Research Laboratories, Eindhoven.

His research interest lies in signal processing for illumination systems, digital communications, and recording systems.

Jan W. M. Bergmans (SM'91) received the Elektrotechnisch Ingenieur (*cum laude*) degree and the Ph.D. degree, both from Eindhoven University of Technology, Eindhoven, The Netherlands, in 1982 and 1987, respectively.

From 1982 to 1999, he was with Philips Research Laboratories, Eindhoven, working on signal processing techniques and IC architectures for digital transmission and recording systems. In 1988 and 1989, he was an exchange researcher with Hitachi Central Research Labs, Tokyo, Japan. Since 1999, he has been Professor and Chairman of the Signal Processing Systems Group, Eindhoven University of Technology. Since 1998, he has been an advisor to the Data Storage Institute, Singapore, and since 2000, to Philips Research Laboratories, Eindhoven. He has published extensively in refereed journals, has authored the book *Digital Baseband Transmission and Recording* (Boston, MA: Kluwer Academic, 1996), and holds approximately 40 U.S. patents.

Tim C. W. Schenk (S'01–M'07) received the M.Sc. and Ph.D. degrees in electrical engineering from Eindhoven University of Technology (TU/e), Eindhoven, The Netherlands, in 2002 and 2006, respectively.

From 2002 to 2004, he was with the Wireless Systems Research Group, Agere Systems, Nieuwegein, The Netherlands. From 2004 to 2006, he was a Research Assistant with the Radiocommunications Group, TU/e. Currently, he is with Philips Research Laboratories, Eindhoven, as a Senior Scientist and Cluster Leader in the Distributed Sensor Systems Department. His research interests include applied signal processing, wireless optical communications, and networked control systems. He authored the book *RF Imperfections in High-Rate Wireless Systems: Impact and Digital Compensation* (The Netherlands: Springer, 2008), and numerous scientific publications in the field of signal processing and communications. He is inventor of over 30 patents and patent applications.

Dr. Schenk was awarded the 2006 Veder Award from the Dutch Scientific Radio Fund Veder for his contributions in the field of system optimization for multiple-antenna systems.